A Hybrid Coordinated Design Method for Power System Stabilizer and FACTS Device Based on Synchrosqueezed Wavelet Transform and Stochastic Subspace Identification

Ayda Faraji, Ali Hesami Naghshbandy, and Arman Ghaderi Baayeh

***Abstract*—The occurrence of low-frequency electromechanical oscillations is a major problem in the effective operation of power systems. The scrutiny of these oscillations provides substantial information about power system stability and security. In this paper, a new method is introduced based on a combination of synchrosqueezed wavelet transform and the stochastic subspace identification (SSI) algorithm to investigate the low-frequency electromechanical oscillations of large-scale power systems. Then, the estimated modes of the power system are used for the design of the power system stabilizer and the flexible alternating current transmission system (FACTS) device. In this optimization problem, the control parameters are set using a hybrid approach composed of the Prony and residual methods and the modified fruit fly optimization algorithm. The proposed mode estimation method and the controller design are simulated in MATLAB using two test case systems, namely IEEE 2-area 4-generator and New England-New York 68-bus 16-generator systems. The simulation results demonstrate the high performance of the proposed method in estimation of local and inter-area modes, and indicate the improvements in oscillation damping and power system stability.**

***Index Terms*—Low-frequency oscillation, modified fruit fly optimization algorithm, Prony analysis, stochastic subspace identification (SSI) algorithm, synchrosqueezed wavelet transform (SSWT).**

I. Introduction

NOWADAYS, low-frequency electromechanical oscillations (LFEOs) with poor or negative damping have become a significant threat to power system stability. It is vital to analyze these oscillations to achieve the stability and security of power system [1]. Two basic methods are available for the computation of modes: model-based and measurement-based methods [2]. Since power systems are time-varying and nonlinear, it is infeasible to model all components in detail and laborious to forecast power interchange. In recent years, wide-area measurement-based approaches have been used more widely [3]. Therefore, a key component of power system development is the deployment of measurement systems, which is generally referred to as the synchrophasor technology [4]. Moreover, there is an electronic device, i.e., phasor measurement unit (PMU), that records sophisticated digital signal and provides synchrophasors using three-phase alternating current (AC) and/or voltage waveforms [5], [6]. PMU uses state-of-the-art digital signal processors that can measure single-phase and three-phase AC waveforms. For digitization, a fixed sampling rate is used with a synchronized global positioning system (GPS) clock. Afterward, these devices communicate the synchronized dynamic data of power system [7].

There are two categories for the classification of typical data, including ambient and ring-down data. Ambient data are aggregated from a power system under stable conditions without any major disruption, and the perturbation results from load changes [8]. After a significant disturbance such as generator or load tripping, the ring-down data emerge as observable oscillations in the system variables. On the other hand, the information of power system modes is not transported using non-typical data including outliers and missing data [9]. Eigenvalue estimation methods are grouped as either block processing or recursive methods. In a block processing method, the estimation is accomplished on a data window. However, in a recursive method, the modes are calculated using the last measured sample and the previous data window [10].

Several mode estimation methods have been reported. Block processing methods such as the Fourier transform [11] and Prony [12], [13] methods, are enforceable solely on ring-down data. In recent research, some block processing algorithms have been expanded for ambient data, including stochastic subspace identification (SSI) algorithm [14]. For the mode estimation of ambient and ring-down data, however, the Kalman filtering [15], recursive least squares (RLS) [16], and wavelet transform (WT) [17] methods can be used. Then, a recursive method called auto-regressive moving aver-

Manuscript received: July 24, 2019; accepted: May 28, 2020. Date of Cross-Check: May 28, 2020. Date of online publication: October 1, 2020.

A. Faraji, A. H. Naghshbandy (corresponding author), and A. G. Baayeh are with the Department of Electrical Engineering, Faculty of Engineering, University of Kurdistan, Sanandaj, Kurdistan, Iran (e-mail: a.faraji@eng.uok.ac.ir; hesami@uok.ac.ir; arman.ghaderi@gmail.com).

DOI: 10.35833/MPCE.2019.000496

age exogenous (ARMAX) is applied to the ambient response [18]. Recursive maximum likelihood [19] and Hilbert-Huang transform [20] are other remarkable methods in this regard. Recently, a noteworthy field in signal processing is the time-frequency analysis, which generally pertains to the analysis of non-stationary signals. Reference [21] presents a new time-frequency analysis method referred to as synchrosqueezed wavelet transform (SSWT). The SSWT calculation is not intricate. After applying the wavelet transform to the signal, the frequency associated with each scale is determined using the derivative of the wavelet transform coefficients with respect to the shift factor. The above steps drastically revise the time-frequency resolution [22]. Currently, SSWT has been applied in civil engineering for low-frequency oscillation analysis [23] and other fields of science, which has obtained acceptable results.

A variety of methods have been introduced for controller design. Several control strategies have been proposed for the coordinated design of the power system stabilizer (PSS) and flexible alternating current transmission system (FACTS) device parameters through system models. These models include linear matrix inequality (LMI), H_∞, optimal, adaptive, and robust controllers [24], and the multi-objective optimization methods used include the genetic algorithm, particle swarm optimization (PSO), and neural networks [25], [26]. However, with the progress in wide-area monitoring, signal processing, and optimization techniques, the application of measurement-based methods has been considered extensively [27]-[29].

In this paper, the proposed SSWT-SSI method estimates the eigenvalues aided by the assembled data of the power system, which is a hybrid of SSWT and SSI. Then, the control parameters are designed using Prony and residual methods. The modified fruit fly optimization algorithm (MFOA) is used to improve the damping and dynamic performances and to meet the constraints of the PSS and FACTS parameters.

The remainder of this paper is organized as follows. Section II provides a brief description of the SSWT and SSI algorithms and some problems concerning the algorithm implementation, mode estimation, and transfer function calculation using the Prony method. In Section III, the proposed design method is used for the explanation of the control parameter tuning with the MFOA. Section IV presents the simulation results on 2-area 4-generator and 68-bus 16-generator IEEE test systems. Finally, conclusions are drawn in Section V.

II. Estimation of Low-frequency Modes and Residue Values

The wavelet coefficients $W_s(a, b)$ of the studied signal $f(t)$ are acquired using the continuous wavelet transform (CWT):

$$W_s(a,b)=\int_{-\infty}^{\infty} f(t)a^{-\frac{1}{2}}\psi((t-b)/a)\mathrm{d}t \tag{1}$$

where a is the scale factor, which is inversely related to frequency; and b is the shift factor associated with time. In the small-scale factor, a wavelet indicates time density, which measures the details of the high-frequency signal. In the large-scale factor, on the contrary, a wavelet represents time expansion, which analyzes the approximations of the low-frequency signal. The complex conjugate of the mother wavelet $\psi(t)$ is $\psi^*(t)$, which is selected as Morlet wavelet. $\omega_s(a,b)$ can be obtained by using the partial derivative of $W_s(a,b)$ according to instantaneous frequency b [21] as:

$$\omega_s(a,b)=-i(W_s(a,b))^{-1}\partial(W_s(a,b))/\partial b \tag{2}$$

In (2), a, b, and ω are discretized. $W_s(a,b)$ is calculated at a discrete a_k, and the reconstruction is determined via inverse transformation of $T_s(\omega_1,b)$:

$$f(b)\approx \mathrm{Re}\left[C_\psi^{-1}\sum_l T_s(\omega_l,b)\Delta\omega\right] \tag{3}$$

where $T_s(a,b)$ is the synchrosqueezed transform, which is obtained at the center frequency ω_l; $\Delta\omega=\omega_l-\omega_{l-1}$; and C_ψ is the Fourier transform of ψ [22], [23].

The data reconstructed for each mode are placed into a block Hankel matrix based on the SSI method, and the SVD of the weighted projection is calculated. Finally, mode damping and frequency can be obtained from the eigenvalue analysis of the state matrix [14].

After the estimation of the modes, the Prony algorithm is used to calculate the residue values. If the power system is represented as a transfer function, the function can be approximated by:

$$G(z)=\frac{\sum_{j=0}^{M} b_j z^{-j}}{\left(1-\lambda_1 z^{-1}\right)\left(1-\lambda_2 z^{-1}\right)\ldots\left(1-\lambda_N z^{-1}\right)} \tag{4}$$

where λ_i ($i=1,2,\ldots,N$) is the root of the equation; b_j ($j=1,2,\ldots,M$) is the equation coefficients of the zeros of the system; and M and N are the numbers of system zeros and poles, respectively. Finally, the inverse z-transform of $G(z)$, $g(n)$, is given by [12]:

$$g(n)=R_1\lambda_1^n+R_2\lambda_2^n+\ldots+R_N\lambda_N^n \tag{5}$$

where R_i ($i=1,2,\ldots,N$) is the residue value.

III. Controller Design

After calculating the eigenvalues, the residue values, and the transfer function, and the controller parameters can be designed. After the controller is added, the transfer function is composed as $G(s)/(1+\varepsilon h(s)\cdot G(s))$, where $\varepsilon h(s)$ is the transfer function of the controller. The denominator is set to be zero, and since ε and $\Delta\lambda$ are very small, the eigenvalue changes $\Delta\lambda$ can be written as follows:

$$\Delta\lambda=-\varepsilon h(\lambda_m)R_m=-G'(\lambda_m)R_m \tag{6}$$

where $\varepsilon h(\lambda_m)=G'(\lambda_m)$ is the transfer function of the controller; and R_m is the residue pertaining to eigenvalue λ_m. Therefore, we can obtain:

$$\left|G'(s)\right|\Big|_{s=\mathrm{j}\omega_{dm}}=\left|\Delta\lambda_m\right|\Big/\left|R_m\right| \tag{7}$$

$$\arg G'(s)|_{s=\mathrm{j}\omega_{dm}}=\arg\Delta\lambda_m-180^\circ-\arg R_m \tag{8}$$

where $\arg G'(s)$ and $\arg R_m$ are the phases of $G'(s)$ and R_m, respectively; and $j\omega_{dm}$ is the imaginary part of the complex eigenvalue λ_m.

After proper selection of $\Delta\lambda_m$, the controller transfer function can be obtained, and the internal parameters can be calculated in accordance with the structures of the PSSs and unified power flow controller (UPFC) devices [20], [24].

Because of some limitations in the structures of generators and their exciter systems in recent years, PSS and FACTS have been used simultaneously. These tools are the most important and economical controllers to improve the dynamic performance and small-signal stability of the power system, and they are essential to increase the damping of the local and inter-area modes of the power system. An important point of using FACTS devices is to find their desirable locations and select the best input signal, which is possible through examination of the controllability and observability of the estimated modes [30] and [31]. In [32], a controllability index is used for the optimal placement of FACTS controllers. The proposed algorithm for signal estimation and controller design is described in Fig. 1.

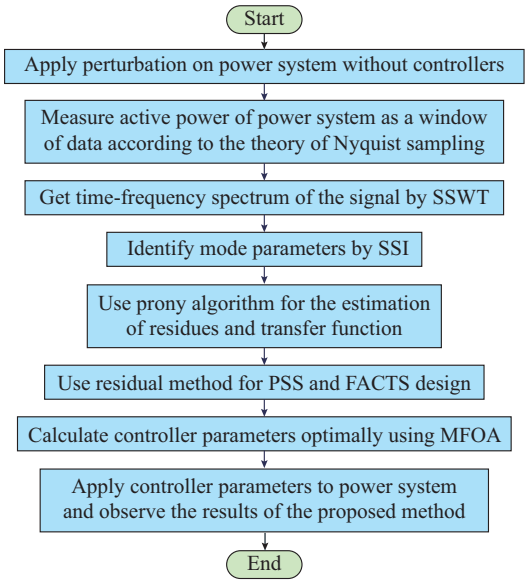

Fig. 1. Proposed algorithm for signal estimation and controller design.

The purpose of this paper is to improve mode damping by examining the search space of the control parameters. The method used in this research is the MFOA, which is a metaheuristic algorithm based on the olfactory search process inherent in fruit flies' foraging behavior. Fruit flies have much stronger senses of smell and vision than other insects, and this helps them find food sources [33], [34].

In this paper, the PSSs are considered with two inputs. The PSS schematic model and the block diagram of UPFC dynamic model are shown in Fig. 2. In a UPFC, two voltage source converters, VSC1 and VSC2, inject active and reactive power, respectively, into bus 1 and the series transformer. The PSS parameters that are determined by the MFOA include the time constants T_1-T_8 and the gains K_{s1}-K_{s3}. Time constants T_{w1}-T_{w4} are invariant. The parameters of UPFC comprise the gains and time constants T_{rv}, T_{rp}, and T_{rq}.

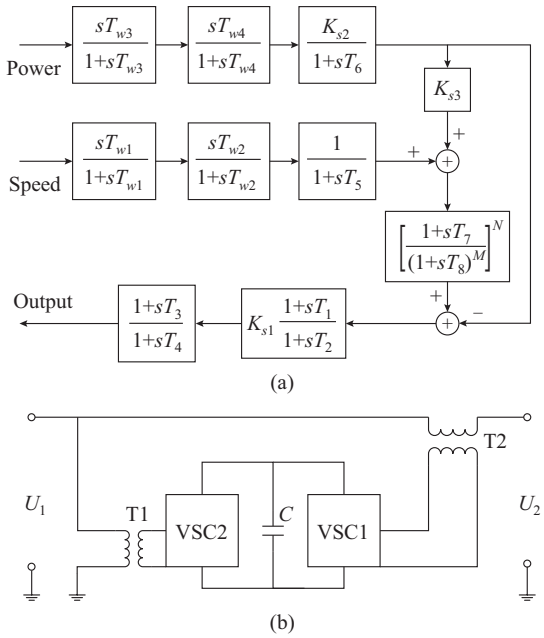

Fig. 2. Structure of controllers. (a) Schematic model of PSS with two inputs. (b) UPFC schematic model.

The objective function is defined as follows. If the system is unstable, the function value will increase, and the value of the objective function will be reduced through the improvement of the system damping (the real parts of the eigenvalues should be negative).

$$\min_{K_s, T_1, T_2, T_3, T_4} F = \sum_{i=1}^{e} e^{\mathrm{Re}[\lambda_{newi}]} \tag{10}$$

where λ_{newi} is the i^{th} eigenvalue of the system after applying the controllers; u is the number of UPFCs; and e is the number of eigenvalues in the power system under investigation.

The inequality and equality constraints defined for the specification of the optimal parameters can be written using (7) and (8). As a result, the equality constraints are:

$$g_i(x) = \left\{ \left| T_{con} \right| \right\} - \left| \frac{\lambda_{new_i} - \lambda(i)}{R(i)} \right| = 0 \tag{11}$$

$$g_{i+1}(x) = \{\arg(T_{con})\} - \arg(\lambda_{new_i} - \lambda(i)) - \pi - \arg(R(i)) = 0 \tag{12}$$

where $T_{con} = \prod_{j=1}^{p} \left\{ \left| T_{pss_j} \right| \right\} + \sum_{m=1}^{u} \left\{ \left| T_{upfc_m} \right| \right\}$, T_{pss} is the transfer function of the PSS, T_{upfc} is the transfer function of the UPFC, and u is the number of UPFC; p is the number of generators with PSSs; $\lambda(i)$ and $R(i)$ are the eigenvalues and residual values calculated using the proposed method, respectively; and the eigenvalues λ_{new_i} are state variables. The inequality constraints are applied to the PSS parameters including T_1-T_8, K_{s1}-K_{s3}, and the parameters of UPFC including K_{UPFC}, T_{rv}, T_{rp}, and T_{rq}. The importance of the proposed method (SSWT-SSI) concerns the precise estimation of the eigenvalues $\lambda(i)$ and residue values $R(i)$, and this method is very accurate compared with the other examined methods, as mentioned above.

IV. Simulation Results

A. 2-area 4-generator Test System

In various studies on mode estimation, several types of disturbance have been investigated for the examination of small-signal stability. The favorable disruption would include different operation conditions such as different faults at various locations, e.g., three-phase faults, loss of line, and changes in the exciter reference voltage of generators and load amounts, and the noise behavior of the load. Two types of disturbance are applied to two systems below for investigating the effectiveness of the proposed method, and consequently, the estimation of modes. The first examined system is the 2-area 4-generator system. Figure 3(a) shows the single-line diagram of the system.

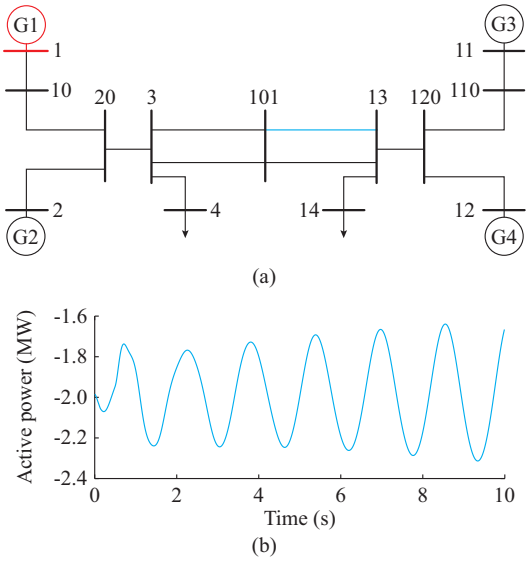

Fig. 3. Single-line diagram and active power signal of 2-area 4-generator test system. (a) Single-line diagram. (b) Active power passing through transmission line 101-13.

It is assumed that all the four generators are equipped with PSSs [1]. To create the disturbance in the system, a step change of 0.05 p.u. is applied in the field voltage at generator 1, which is marked in red in Fig. 3(a). A measured data window of active power flow, which has ten seconds with the 50 Hz sampling rate on the transmission line 101-13 marked in blue in Fig. 3(a), is used for estimation of the modes as shown in Fig. 3(b). First, the DC component is removed. The examined signal is transformed by SSWT and Fig. 4(b) illustrates its time-frequency distribution. For demonstrating the credit of SSWT, all the intrinsic mode type (IMT) components (IMT1-IMT4) are reconstructed, as shown in Fig. 4(a). Clearly, the energy distribution in each mode varies with time, as illustrated in Fig. 4(a). The frequency and the damping of the modes are presented in Table I. The signal reconstructed using the proposed hybrid method is shown in Fig. 5. The error percentage of the reconstructed signal is less than 2%, which is calculated using the Euclidean norm.

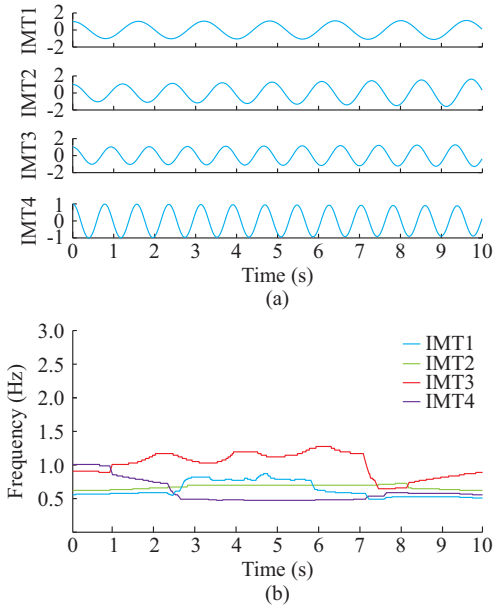

Fig. 4. Reconstruction of IMT and time-frequency analysis. (a) Reconstruction of IMT. (b) Time-frequency analysis result.

TABLE I
Estimation of Eigenvalues, Damping, and Frequency Using Proposed Method for 2-area 4-generator System

Frequency (Hz)	Damping	Eigenvalue	Residue value
0.624240	–0.011910	±j3.9222 + 0.0467	–0.0695 – j0.0748
0.822424	–0.050190	±j5.1674 + 0.2597	0.0023 + j0.0015
1.071326	–0.025080	±j6.7313 + 0.1689	–0.0009 + j0.0005
1.278623	0.012218	±j8.0338 – 0.0982	0.0099 – j0.0020

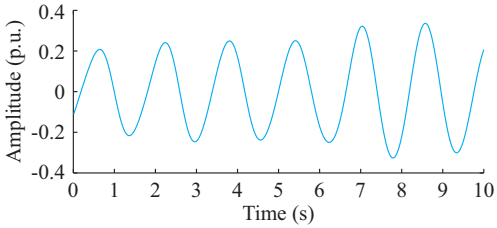

Fig. 5. Reconstituted signal.

To verify the accuracy and validate the SSWT-SSI method, the estimated eigenvalues are compared with those calculated by the modal, CWT, and SSI methods through the calculation of the signal-to-noise ratio (SNR) in Table II. As can be observed, all the three have rates higher than 40 dB, while the SSWT-SSI method with SNR = 61.7516 dB provides the most accurate eigenvalue estimation. All the three methods have anti-noise capability.

The SSI method is highly dependent on the selected system order and nonlinear elements, and the CWT method, like the SSWT method, requires human participation when the mode is estimated with the image observation method. However, these problems are resolved aided by the SSWT-SSI method, and the estimation speed increases.

In this paper, we try to apply a disturbance to the power system to demonstrate the effectiveness of the proposed

method in handling small-signal stability and controller design. It is noted that the SSWT-SSI method is flexible for studying both stationary and non-stationary signals. Furthermore, given that the Prony and SSI methods alone are not suitable for investigating non-stationary signals, we select some disturbances that exhibit non-stationary behavior. The mode estimation capability of the presented method can thus be observed. Therefore, the selected signal in the 2-area 4-generator test system is stationary, and the signal in the 68-bus 16-generator test system is non-stationary. Moreover, SSI, CWT, and SSWT methods have anti-noise capability.

TABLE II
COMPARISON OF DETECTED EIGENVALUES USING SSWT-SSI, MODAL, SUBSPACE, AND CWT METHODS

No.	Eigenvalue of SSWT-SSI	Eigenvalue of modal	Eigenvalue of subspace	Eigenvalue of CWT
1	±j3.9222+ 0.0467	±j3.9226+ 0.0671	±j3.7213+ 0.0454	±j4.0099+ 0.0552
2	±j5.1674+ 0.2597	±j4.8671+ 0.4591	±j5.0677+ 0.2578	±j5.2654+ 0.3787
3	±j6.7313+ 0.1689	±j7.1321+ 0.1082	±j6.6281+ 0.1688	±j6.9933+ 0.0701
4	±j8.0338– 0.0982	±j8.0333– 0.0988	±j8.2325– 0.0871	±j7.9351– 0.1073
SNR (dB)	61.7516	57.0019	58.8049	60.5961

Figure 6 shows the results of frequency-time analysis at two different noise levels (10 dB and 15 dB).

The above analysis demonstrates that SSWT has anti-noise capability, particularly for frequency performance against noise, to a certain degree. However, the other methods such as the Prony and SSI methods are not robust against noise, requiring de-noising, and this problem is resolved aided by the SSWT method.

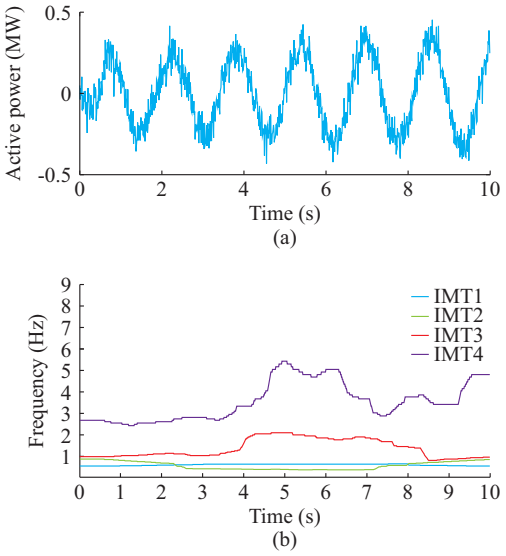

Fig. 6. Frequency-time analysis of signal obtained by SSWT with noise. (a) Signal at noise level of 10 dB. (b) Time-frequency analysis at noise level of 15 dB with SSWT.

After the high-accuracy estimation of the eigenvalues, residuals, and transfer function using the proposed method, (11) and (12) are solved by MFOA, and the calculated PSS parameters of generators 1 and 3 are presented in Table III.

TABLE III
PSS PARAMETERS OF GENERATORS 1 AND 3 IN 2-AREA 4-GENERATOR TEST SYSTEM WITH SSWT-SSI METHOD

Generator No.	K_{s1}	K_{s2}	K_{s3}	T_1	T_2	T_3	T_4	T_5	T_6	T_7	T_8
G1	92	89	92	0.0764	0.0122	0.0607	0.0127	0.0774	0.0125	0.0745	0.0137
G3	93	88	92	0.0667	0.0135	0.0674	0.0125	0.0774	0.0135	0.0774	0.0135

In Fig. 7, the active power flow of the transmission line 101-13 is illustrated in the presence and absence of the PSS, the parameters of which are designed based on the proposed, modal, and CWT-Prony methods, respectively. The rotor angle waveforms of generator 3 are compared in four cases in Fig. 8, without and with PSS parameters as designed by SSWT-SSI, modal, and CWT-Prony methods, respectively. The results show the efficiency and proper performance of the SSWT-SSI method for improvement of the stability and oscillation damping of the system.

B. 68-bus 16-generator Test System

In this section, the performance of the SSWT-SSI method is studied on a 68-bus 16-generator test system. The single-line diagram of the system is presented in Fig. 9(a). The system has 86 transmission lines and 16 generators, where generators 13 to 16 are area-equivalents, and PSSs cannot actually be placed in them. The results of the controllability index calculations in [29] show that the optimal location of the UPFC in the five-area system is at line 46-49, followed by line 50-51, and the results of the observability index calculations demonstrate that the optimal location of the PMU in the five-area system is at line 17-27 [31]. Thus, it is assumed that the UPFC is installed between buses 46 and 49, and for examination of the 68-bus 16-generator test system, the active power flow passing through the 17-27 transmission line, which is marked in blue in Fig. 9(a), is selected as data window, as shown in Fig. 9(b).

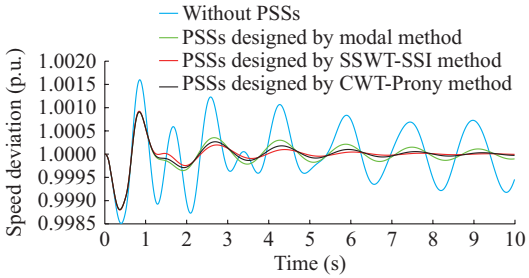

Fig. 7. Comparison of active power of line 101-13 in presence of controllers designed by modal, CWT-Prony, and SSWT-SSI methods and in absence of PSSs.

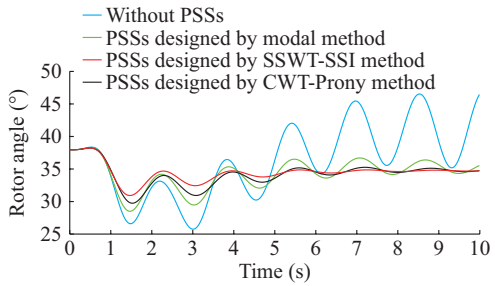

Fig. 8. Comparison of rotor angle waveforms with controllers designed by different methods.

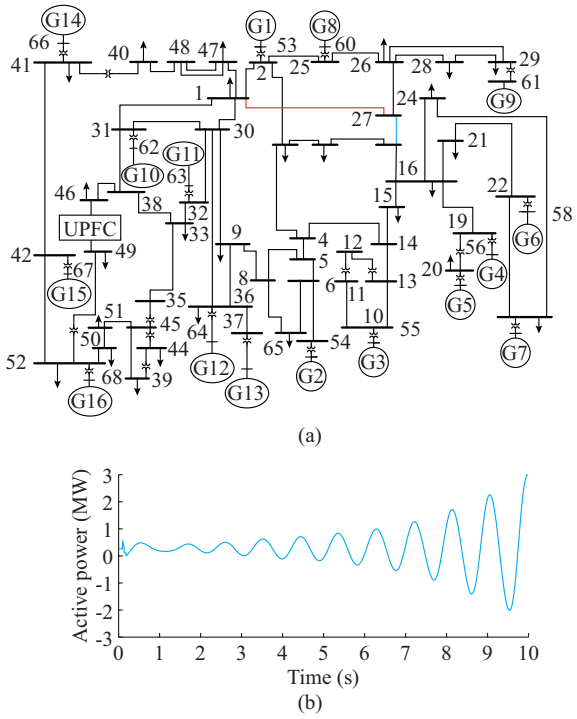

Fig. 9. Single-line diagram of 68-bus 16-generator system and active power signal. (a) Single-line diagram of 68-bus 16-generator test system. (b) Active power through line connecting buses 17 and 27.

For creating a perturbation, a three-phase fault is applied to the line connected between buses 1 and 27, which is marked in red in Fig. 9(a) [29]. The sampling rate of 40 Hz is considered based on the Nyquist sampling theory. The SSWT method is applied to the active power flow of the transmission line 17-27, and the obtained time-frequency spectrum is illustrated in Fig. 10. In Fig. 10(a), it is clear that the energy distribution in each mode varies with time and frequency. The frequency and damping and residue values are estimated. After the estimation, it can be seen that the energy of the oscillation mode 0.6523 Hz is gradually reduced, while the energy of the other two modes gradually increases.

The reconstructed signal is shown in Fig. 11(a). Figure 1l(b) illustrates the error percentage involving a comparison of the reconstructed and the actual signal. The error percentage of the reconstructed signal is less than 2%.

The frequency and damping of the first to third modes and residue values are given in Table IV. The SNRs of SSWT-SSI and CWT methods are 56.7827 dB and 55.3515 dB, respectively.

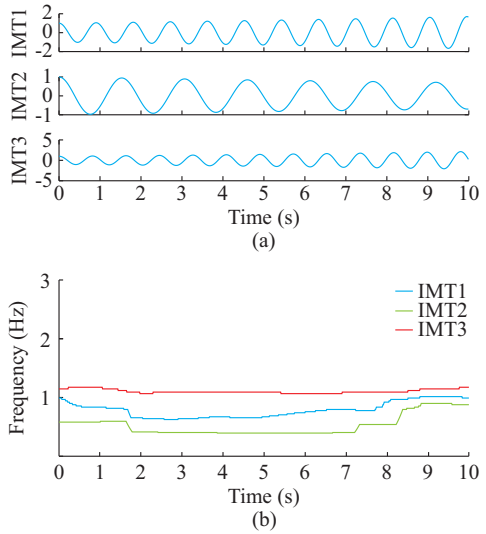

Fig. 10. Reconstruction of IMT and time-frequency spectrum. (a) Reconstruction of IMT. (b) Time-frequency spectrum analysis with SSWT-SSI.

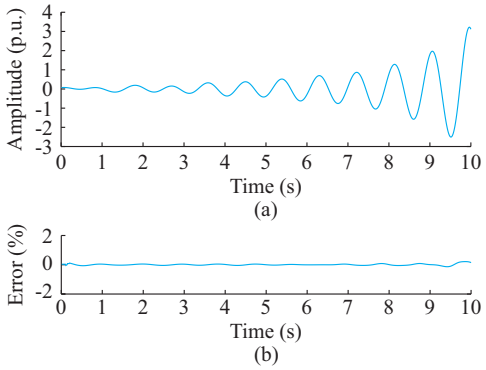

Fig. 11. Reconstituted signal and error waveform. (a) Reconstituted signal. (b) Signal reconstruction error.

TABLE IV
EIGENVALUES, DAMPING, AND FREQUENCY IDENTIFIED USING PROPOSED AND CWT METHODS IN 68-BUS 16-GENERATOR TEST SYSTEM

SSWT-SSI method			CWT method
Frequency (Hz)	Damping	Eigenvalue	Eigenvalue
0.6523*	0.0359*	−0.1472±j4.0985	−0.1368±j4.1068
1.1052**	−0.0533**	+0.3707±j6.9442	+0.3913±j6.8435
1.2244**	−0.0771**	+0.5949±j7.6931	+0.5969±j7.6941

Note: * means the damping ζ is in the range of $0 \le \zeta < 0.1$ and ** means $\zeta <$ 0.

To validate the accuracy of the proposed method, its estimated eigenvalues are compared with those obtained by the modal method. The comparison shows that the SSWT-SSI method is more accurate. After the transfer function is identified, the controller parameters are specified using the method of this paper.

The controller parameters are given in Table V. The speed deviation waveforms of generators 1-12 in the presence of PSS and UPFC are illustrated in Fig. 12. Here, the controllers are designed with three different methods, including the modal, CWT-Prony, and SSWT-SSI methods. The results of

the power system simulation indicate the better performance of the SSWT-SSI method in improvement of the stability of the 68-bus 16-generator test system. Figure 13(a) shows the waveforms of the active power passing through the transmission line 17-27 with and without controllers. The estimated eigenvalues of the system before and after setting the controllers are compared in Fig. 13(b) and Fig. 13 (c), respectively. The black, green, and red dots mean $\zeta>0$, $0.1<\zeta<0.2$, and $\zeta<0$, respectively.

TABLE V
PARAMETERS OF PSSS AND UPFC IN 68-BUS 16-GENERATOR TEST SYSTEM

Item	Parameters
G1	$K_{s1}=92$, $K_{s2}=89$, $K_{s3}=95$, $T_1=0.0764$, $T_2=0.0122$, $T_3=0.0707$, $T_4=0.0102$, $T_5=0.0674$, $T_6=0.0102$, $T_7=0.0727$, $T_8=0.0147$
G3	$K_{s1}=91$, $K_{s2}=91$, $K_{s3}=93$, $T_1=0.0664$, $T_2=0.0122$, $T_3=0.0607$, $T_4=0.0107$, $T_5=0.0766$, $T_6=0.0112$, $T_7=0.0674$, $T_8=0.0140$
UPFC	$T_{rp}=0.147$, $K_{pp}=1.902$, $K_{ip}=2.271$, $T_{rq}=0.303$, $K_{pq}=1.102$, $K_{iq}=1.852$, $T_{rv}=0.651$, $K_{pv}=1.356$, $K_{iv}=2.444$

Note: K_{pp}, K_{ip}, K_{pq}, K_{iq}, K_{pv}, and K_{iv} are the gains of UPFC.

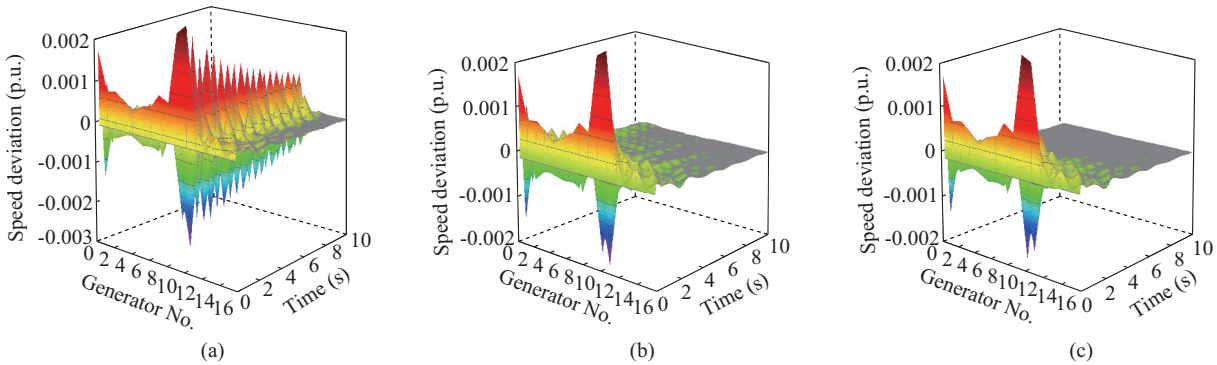

Fig. 12. Comparison of generator speed deviations obtained through application of controller design using different methods. (a) Modal method. (b) CWT-Prony method. (c) SSWT-SSI method.

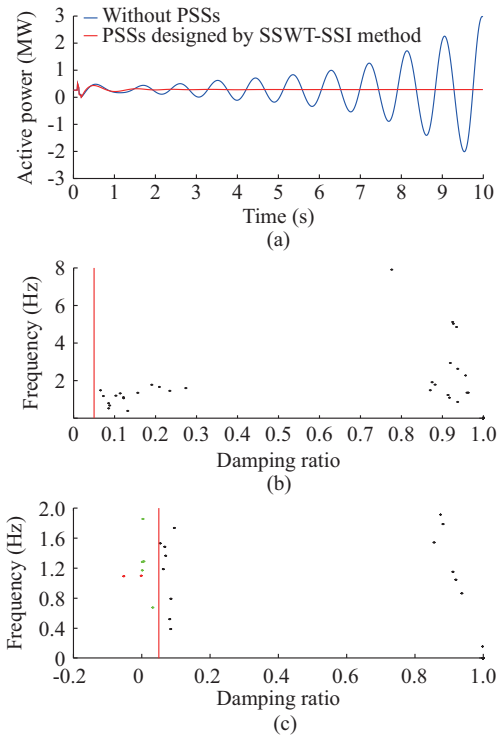

Fig. 13. Comparison of eigenvalues of 68-bus 16-generator test system before and after application of controllers. (a) Comparison of active power waveforms in two cases with and without controllers. (b) Eigenvalues of system with controllers. (c) Eigenvalues of system without controllers.

The modes are calculated using the SSWT-SSI, CWT-Prony, and modal methods when the controllers are applied to the 68-bus 16-generator test system. The results are shown in Table VI. As can be seen, the damping of the modes is improved when the PSSs and UPFC are designed by the methods based on wavelet transform. All the obtained modes of the SSWT-SSI method have damping of more than 0.1, and those of the CWT-Prony method have damping of more than 0.1, and there is only one mode with $0.1\le\zeta<0.2$, indicated by star. However, the modes obtained from the modal method have poor damping $0\le\zeta<0.1$ and $\zeta<0$, shown by star and double stars, respectively. Thus, the SSWT-SSI method is successfully applied to establish the optimal coordination between PSSs and UPFC as supplementary damping controllers (SDCs). The rotor angle waveforms of generator 1 are compared in Fig. 14, in four cases: without the PSS parameters and with them as designed by the SSWT-SSI, modal, and CWT-Prony methods.

TABLE VI
COMPARISON OF MODES AFTER DESIGN OF CONTROLLERS USING SSWT-SSI, CWT-PRONY, AND MODAL METHODS IN 68-BUS 16-GENERATOR TEST SYSTEM

SSWT-SSI method		CWT-Prony method		Modal method	
Frequency (Hz)	Damping	Frequency (Hz)	Damping	Frequency (Hz)	Damping
0.6381	0.2359	0.62230	0.2385	0.6223*	0.1985*
1.0052	0.2038	1.00320*	0.1933*	1.0032	0.2933
1.3244	0.6071	1.38244	0.5997	1.1924**	–0.0089**

Note: * means $0.1\le\zeta<0.2$ and ** means $\zeta<0$.

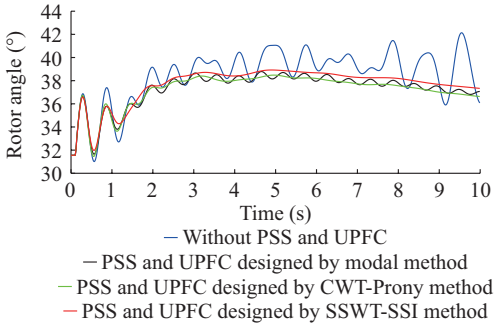

Fig. 14. Comparison of rotor angle of G1 in four cases without controllers and with PSSs and UPFC as designed by three methods.

In both two disturbances to study the 68-bus 16-generator test system, the active power flow on the line connected between buses 17 and 27 is considered as a window of measured data for analysis. Then, the time-frequency distribution analysis plots by SSWT have been obtained. The frequency and damping of the modes in both two cases are given in Table VII.

TABLE VII
IDENTIFIED FREQUENCY AND DAMPING WITH LOAD AT BUS 1 LOST AND 3-PHASE FAULT APPLIED TO LINE 1-2 IN 68-BUS 16-GENERATOR TEST SYSTEM USING SSWT-SSI METHOD

No.	Loss of load at bus 1		3-phase fault to line 1-2	
	Frequency (Hz)	Damping	Frequency (Hz)	Damping
1	0.4119*	0.0908*	0.5355*	0.0444*
2	0.8965*	0.0090*	1.0192*	0.0897*
3	1.3201**	−0.0117**	1.5055*	0.0444*

Note: * means $0 \le \zeta < 0.1$ and ** means $\zeta < 0$.

After the calculation of the eigenvalues and residue values, the control parameters are determined. Figure 15 shows the active power waveforms on the tie line connected between buses 17 and 27 in two cases without and with PSSs and UPFC designed by SSWT-SSI.

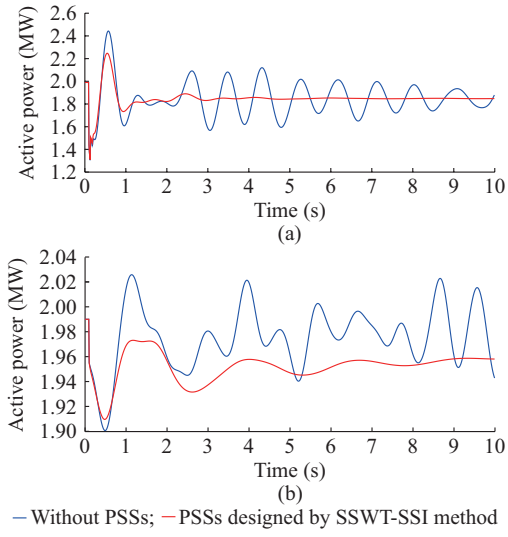

Fig. 15. Comparison of active power waveforms of line 17-27 with two different faults. (a) Comparison of active power in two cases with and without controllers when load at bus 1 is lost. (b) Comparison of active power waveforms in two cases with and without controllers when applying 3-phase fault to line 1-2.

It should be noted that this method is suitable for investigating both types of data, including ambient and ringdown data, although the ringdown data measured after a major disturbance are used to study the small-signal stability as presented in this paper.

V. CONCLUSION

In this paper, a new method of time-frequency analysis is presented to estimate low-frequency oscillation modes, residue values, and transfer function of power system. The proposed method is a combination of the SSWT, SSI, and Prony methods.

The SSWT method overcomes the problems of energy deviation and mode mixing in WT. Moreover, the method improves the accuracy of identification of the examined oscillations with better anti-noise performance. The combination of SSWT and SSI presents an automatic identification algorithm, thus, the mode prediction occurs before signal reconstruction, and parameter identification becomes effective. The use of the Prony method provides a better estimation of the signal transfer function. For setting the PSSs and UPFC parameters, the equations are obtained from the residual method and solved using MFOA. This optimization algorithm is used to increase the design accuracy, and ultimately, generates parameters that are consistent with the practical limits.

The simulations of two well-known systems, namely the 2-area 4-generator and the 68-bus 16-generator test systems, verify the high performance and efficiency of the SSWT-SSI method. The results also demonstrate a considerable increase in the damping of LFEOs. For comparing the capability of the proposed algorithm and the other methods, the advantages of the hybrid algorithm are briefly presented as follows.

1) A window of data is used as measured signal.
2) The proposed method is robust against noise.
3) The speed and accuracy of calculation for estimation of modes is increased by the proposed automatic method and MFOA.
4) The optimal controller parameters is calculated given the practical ranges.
5) The damping and stability are increased in the power system.

REFERENCES

[1] A. R. Messina, "Advanced data processing and feature extraction," in *Wide-area Monitoring of Interconnected Power Systems*, Stevenage: The IET Press, 2015, pp. 63-96.
[2] J. Turunen, J. Thambirajah, M. Larsson *et al.*, "Comparsion of three electromechanical oscillation damping estimation methods," *IEEE Transactions on Power Systems*, vol. 26, no. 4, pp. 2398-2407, Nov. 2011.
[3] S. You, J. Guo, G. Kou *et al.*, "Oscillation mode identification based on wide-area ambient measurements using multivariate empirical mode decomposition," *Electric Power Systems Research*, vol. 134, pp. 158-166, May 2016.
[4] A. Chakraborttyl and P. P. Khargonekar, "Introduction to wide-area control of power systems," in *Proceedings of American Control Conference*, Washington DC, USA, Jun. 2013, pp. 1-13.
[5] A. Chakrabortty, J. H. Chow, and A. Salazar, "A measurement-based framework for dynamic equivalencing of large power systems using wide-area phasor measurements," *IEEE Transactions on Smart Grid*, vol. 2, no. 1, pp. 68-81, Mar. 2011.

[6] M. Weiss, A. Chakrabortty, and F. Habibi Ashraf, "A wide-area SVC controller design using a dynamic equivalent model of WECC," in *Proceedings of IEEE PES General Meeting*, Denver, USA, Jul. 2015, pp. 1-5.
[7] M. U. Usman and M. O. Faruque, "Applications of synchrophasor technologies in power systems," *Journal of Modern Power Systems and Clean Energy*, vol. 7, no. 2, pp. 211-226, Mar. 2019.
[8] C. Chen, Z. An, X. Dai *et al*., "Measurement-based solution for low frequency oscillation analysis," *Journal of Modern Power Systems and Clean Energy*, vol. 4, no. 3, pp. 406-413, May 2016.
[9] A. Zamora, V. M. Venkatasubramanian, J. A. Serna *et al*., "Multi-dimensional ringdown modal analysis by filtering," *Electric Power Systems Research*, vol. 143, pp. 748-759, Feb. 2017.
[10] C. Huang, F. Li, D. Zhou *et al*., "Data quality issues for synchrophasor applications part I: a review," *Journal of Modern Power Systems and Clean Energy*, vol. 4, no. 3, pp. 342-352, Jul. 2016.
[11] H. Wen, J. Zhang, W. Yao *et al*., "FFT-based amplitude estimation of power distribution systems signal distorted by harmonics and noise," *IEEE Transactions on Power Systems*, vol. 14, no. 4, pp. 1447-1455, Sept. 2018.
[12] G. Liu, J. Quintero, and V. M. Venkatasubramanian, "Oscillation monitoring system based on wide area synchrophasors," in *Proceedings of Power Systems iREP Symposium – Bulk Power System Dynamics and Control-VII: Revitalizing Operational Reliability*, Charleston, USA, Aug. 2007, pp. 1-13.
[13] K. H. Jin and L. Yilu, "Identification of interarea modes from an effectual impulse response of ringdown frequency data," *Electric Power Systems Research*, vol. 144, pp. 96-106, Mar. 2017.
[14] S. A. N. Sarmadi and V. Venkatasubramanian, "Electromechanical mode estimation using recursive adaptive stochastic subspace identification," *IEEE Transactions on Power Systems*, vol. 29, no. 1, pp. 349-358, Sept. 2014.
[15] M. Yazdanian, A. Mehrizi-sani, and M. Mojiri, "Estimation of electromechanical oscillation parameters using an extended Kalman filter," *IEEE Transactions on Power Systems*, vol. 30, no. 6, pp. 2994-3002, Jan. 2015.
[16] M. Beza and M. Bongiorno, "A modified algorithm for online estimation of low-frequency oscillations in power system," *IEEE Transactions on Power Systems*, vol. 31, no, pp. 1703-1714, Jun. 2015.
[17] L. Cheng, X. Ji, F. Zhang *et al.*, "Wavelet-based data compression for wide-area measurement data of oscillations," *Journal of Modern Power Systems and Clean Energy*, vol. 6, no. 6, pp. 1128-1140, Jul. 2018.
[18] L. Dosiek and J. W. Pierri, "Estimating electromechanical modes and mode shapes using the multichannel ARMAX model," *IEEE Transactions on Power Systems*, vol. 28, no. 2, pp. 1950-1959, Apr. 2013.
[19] H. Khalid and J. Peng, "Tracking electromechanical oscillations: an enhanced maximum-likelihood based approach," *IEEE Transactions on Power Systems*, vol. 31, no. 3, pp. 1799-1808, May 2015.
[20] Y. Li, D. Yang, F. Liu *et al*., "Coordinated design of local PSSs and wide-area damping controller," in *Interconnected Power Systems Wide-area Dynamic Monitoring and Control Applications*, Verlag Berlin Heidelberg: Springer, 2015, pp. 103-117.
[21] I. Daubechies, J. F. Lu, and H. T. Wu, "Synchrosqueezed wavelet transforms: an empirical mode decompositionlike tool," *Applied and Computational Harmonic Analysis*, vol. 30, no. 2, pp. 243-261, Mar. 2011.
[22] M. H. Rafiei and H. Adeli, "A novel unsupervised deep learning model for global and local health condition assessment of structures," *Engineering Structures*, vol. 156, pp. 598-607, Feb. 2018.
[23] M. Yu, B. Wang, X. Chen *et al*., "Application of synchrosqueezed wavelet transform for extraction of the oscillatory parameters of low frequency oscillation in power systems," *Transactions of China Electrotechnical Society*, vol. 32, no. 6, pp. 14-20, Mar. 2017.
[24] K. Tang, and G. K. Venayagamoorthy, "Damping inter-area oscillations using virtual generator based power system stabilizer," *Electric Power Systems Research*, vol. 129, pp. 126-141, Dec. 2015.
[25] A. Abiee, "An advanced state estimation method using virtual meters," *Journal of Operation and Automation in Power Engineering*, vol. 5, no. 1, pp. 11-17, Sept. 2017.
[26] A. I. Konara, and U. D. Annakkage, "Robust power system stabilizer design using eigenstructure assignment," *IEEE Transactions on Power Systems*, vol. 31, no. 3, pp. 1845-1853, May 2016.
[27] H. Hasanvand, M. R. Arvan, B. Mozafari *et al*., "Coordinated design of PSS and TCSC to mitigate interarea oscillations," *International Journal of Electrical Power & Energy Systems*, vol. 78, pp. 194-206, Jun. 2016.
[28] A. Faraji and A. H. Naghshbandy, "A combined approach for power system stabilizer design using continuous wavelet transform and SQP," *International Transactions on Electrical Energy Systems*, vol. 29, no. 3, pp. 1-18, Mar. 2019.
[29] J. Quintero and V. Venkatasubramanian, "SVC compensation on a real-time wide-area control for mitigating small-signal instability in large electric power systems," in *Proceedings of International Conference on Power System Technology*, Chongqing, China, Oct. 2006, pp. 1-8.
[30] B. K. Kumar, S. N. Singh, and S. C. Srivastava, "Placement of FACTS controllers using modal controllability indices to damp out power system oscillations," *IET Generation, Transmission & Distribution*, vol. 1, no. 2, pp. 209-217, May 2007.
[31] A. Asgari and K. G. Firouzjah, "Optimal PMU placement for power system observability considering network expansion and $N-1$ contingencies," *IET Generation, Transmission & Distribution*, vol. 12, no. 18, pp. 4216-4224, Oct. 2018.
[32] S. Hajforoosh, S. M. H. Nabavi, and M. A. S. Masoum, "Coordinated aggregated-based particle swarm optimisation algorithm for congestion management in restructured power market by placement and sizing of unified power flow controller," *IET Science, Measurement & Technology*, vol. 6, no. 4, pp. 1447-1455, Aug. 2012.
[33] K. Zhang, Z. Shi, Y. Huang *et al*., "SVC damping controller design based on novel modified fruit fly optimisation algorithm," *IET Renewable Power Generation*, vol. 12, no. 1, pp. 90-97, Jan. 2018.
[34] Y. Yu, Z. Mi, X. Zheng *et al*., "Accommodation of curtailed wind power by electric water heaters based on a new hybrid prediction approach," *Journal of Modern Power Systems and Clean Energy*, vol. 7, no. 3, pp. 525-537, May 2019.

Ayda Faraji received the B. S. and M. S. degrees from the University of Kurdistan, Sanandaj, Iran, in 2014 and 2017, respectively, in electrical engineering. She is currently a Ph. D. student at the University of Kurdistan, Sanandaj, Iran. Her main research interests include the dynamic and stability of power systems.

Ali Hesami Naghshbandy received the B. Sc., M. Sc., and Ph. D., degrees from Iran University of Science & Technology, Tehran, Iran, in 1994, 2000, and 2008, respectively. He is currently an Associate Professor of electrical engineering with the University of Kurdistan, Sanandaj, Iran. He has been a member of IEEE PES, CSS and CIGRE. His research interests include power system simulation, dynamics, stability and security.

Arman Ghaderi Baayeh received his B. Sc. degree from the University of Kurdistan, Sanandaj, Iran, in 2014, and the M.Sc. degree from the Iran University of Science & Technology, Tehran, Iran, in 2016. He is currently an Visiting Researcher at the University of Kurdistan, Sanandaj, Iran. His research interests include protective relaying, analysis of electromagnetic transients in transmission and distribution systems, and geomagnetic disturbance analysis of power systems.